

Indirect Detection of Kaluza–Klein Dark Matter

Gianfranco Bertone^a, Géraldine Servant^{b,c}, Günter Sigl^a

^a *GReCO, Institut d’Astrophysique de Paris, C.N.R.S., 98 bis boulevard Arago, F-75014 Paris, France*

^b *Enrico Fermi Institute, University of Chicago, Chicago, IL 60637*

^c *High Energy Physics Division, Argonne National Laboratory, Argonne, IL 60439*

We investigate prospects for indirect detection of Kaluza–Klein dark matter, focusing on the annihilation radiation of the Kaluza–Klein photon $B^{(1)}$ in the Galactic halo, in particular we estimate neutrino, gamma-ray and synchrotron fluxes. Comparing the predicted fluxes with observational data we are able to constrain the $B^{(1)}$ mass (and therefore the compactification scale). The constraints depend on the specific model adopted for the dark matter density profile. For a NFW profile the analysis of synchrotron radiation puts a lower bound on the $B^{(1)}$ mass of the order of $\simeq 500$ GeV.

PACS numbers: 04.50.+h, 12.60.-i, 14.80.-j, 95.35.+d, 96.40.-z

ANL-HEP-PR-02-099, EFI-02-52

I. INTRODUCTION

Over the last thirty years, independent pieces of evidence have accumulated in favor of the existence of *Dark Matter* (DM), indicating that most of the matter of the universe is non baryonic and of unknown nature. Particle physicists have come up with various DM candidates. The most promising and most extensively studied is the so-called *neutralino*, the Lightest Supersymmetric Particle (LSP) which arises in supersymmetric models and is stable in models with conserved R-parity.

Although theoretically well motivated, *neutralinos* are not the only viable DM candidates and it is important to investigate other possibilities arising in extensions of the Standard Model which are not the Minimal Supersymmetric Standard Model (MSSM). For instance, models with compact extra dimensions possess plenty of new states, Kaluza–Klein (KK) particles. Very different types of models with extra dimensions exist, each showing a distinctive phenomenology. In *brane world* scenarios, the Lightest Kaluza–Klein Particle (LKP) is not stable and cannot be a DM candidate. However, in models with *Universal Extra Dimensions* (UED) [1], in which all Standard Model fields propagate in extra dimensions, including fermions, the LKP may be stable if *KK parity* is preserved. *KK parity* is preserved in all models where boundary lagrangians are identical at both orbifold fixed points. Therefore, in this general class of models, the LKP turns out to be stable and was recently shown to be a viable DM candidate [2].

The LKP is likely to be associated with the first KK excitation of the photon, more precisely the first KK excitation of the Hypercharge gauge boson [3], and we will refer to it as $B^{(1)}$. The relic density of $B^{(1)}$ was computed in Ref. [2] where it was shown that if the LKP is to account for DM then its mass (which is inversely proportional to the compactification radius R) should lie in the range 600–1200 GeV which is above any current experimental constraint: In the case of one extra dimension, the constraint on the compactification scale in UED models from precision electroweak measurements is as low as $R^{-1} \gtrsim 300$ GeV [1]. Very recently it was even argued

that this bound can be weakened to $R^{-1} \gtrsim 200$ GeV if one allows a Higgs mass as heavy as $m_H \gtrsim 550$ GeV [4]. This is to be contrasted with another class of models where SM bosons propagate in extra dimensions while fermions are localized in 4 dimensions, in such cases, the constraint on the compactification scale is much stronger ($R^{-1} \gtrsim$ several TeV).

Direct detection of the LKP via its elastic scattering with nuclei in a detector was investigated in Ref. [5, 6]. It was emphasized in [6] that one-ton detectors are needed to probe the expected heavy masses as indicated by the relic density calculation [2] of the LKP and one has to wait for the next generation of direct detection experiments such as GENIUS [7] or XENON [8]. Simultaneously, LHC should probe most of the relevant KK mass parameter space (up to $R^{-1} \sim 1.5$ TeV [9]) and definitely confirm or rule out UED at the TeV scale.

In addition, there are other ways to probe KK DM *indirectly*: As for other Weakly Interacting Massive Particles (WIMPs), the LKP could be detected via the measurement of fluxes of particles coming from its self annihilation. WIMPs annihilate with higher probability in regions where the density of DM is higher, like in the Sun or in the center of the Galaxy. Indirect detection prospects from LKP annihilation in the Sun was investigated in [5, 10]. The idea is to look for a neutrino spectrum which could be detected by IceCube. Annihilation in the Galaxy can give rise to different fluxes: Positron excess from LKP annihilation was investigated in Ref. [5]. While the signal (which could be detected by AMS) is spectacular for KK masses below 500 GeV, it is almost indistinguishable from background for masses above 800 GeV. The photon spectrum was investigated as well in Ref. [5] and is also studied in the present article.

The aim of this paper is to investigate the prospects for indirect detection of KK dark matter, focusing on radiation from the annihilation of such particles in the Galactic halo. In particular we estimate neutrino and gamma-ray fluxes, and the synchrotron radiation from e^+e^- pairs propagating in the Galactic magnetic field. The paper is organized as follows: In section II the density profiles of dark matter in galaxies and in particular

in the Milky Way are presented. Section III discusses the annihilation of $B^{(1)}$ particles and the details of fragmentation of secondary quarks. In section IV we evaluate gamma and neutrino fluxes from the galactic center and compare the predicted fluxes with observations. In section V we estimate the synchrotron radiation from e^+e^- propagating in the Galactic magnetic field and the constraints on the $B^{(1)}$ mass. Finally, results are summarized and discussed in section VI.

II. DARK MATTER PROFILES

In this section we discuss some widely used profile models for the density of dark matter in galaxies, and the corresponding value for the integration along the line of sight in the direction of the Galactic Center (GC).

The choice of the dark matter density profile is crucial when discussing annihilation radiation, because it fixes the normalization of the observed spectrum. Even under the simplifying assumption of a spherically symmetric profile, the uncertainty on the dark matter distribution is such that it is impossible to put model-independent constraints on physical parameters of dark matter particles.

In fact, there is still no consensus about the shape of dark halos. High-resolution N-body simulations suggest the existence of “cusps”, with the inner part of the halo density following a power law $\propto r^{-\gamma}$ with index γ possibly as high as 1.5 (see below). On the other hand observations of rotation curves of galaxies seem to suggest much shallower inner profiles [11] (but other groups claim the impossibility of constraining dark matter with such observations [12]).

For what concerns the Milky Way, the situation is unclear despite the wide range of observational data available. Binney & Evans (BE, 2001) [13] exclude cuspy profiles with $\gamma > 0.3$, with an analysis based on micro-lensing optical depth. Nevertheless Klypin, Zhao & Somerville (KZS, 2001) [14] find a good agreement between Navarro, Frenk, and White (NFW) profiles, $\gamma = 1$, and observational data for the Galaxy and M31. The main difference between the two analysis is in the modelisation of the Galaxy: KZS claim to have taken into account dynamical effects neglected by BE, and to have a “more realistic” description of the bar.

The usual parametrisation for the dark matter halo density is

$$\rho(r) = \frac{\rho_0}{(r/R)^\gamma [1 + (r/R)^\alpha]^{(\beta-\gamma)/\alpha}} \quad (1)$$

In Tab. I we give the values of the respective parameters for some of the most widely used profile models, namely the Kravtsov et al. (Kra, [15]), Navarro, Frenk and White (NFW, [16]), Moore et al. (Moore, [17]) and modified isothermal (Iso, e.g. [18]) profiles.

The dark matter profile in the inner region of the Milky Way is even more uncertain: observations of velocity dis-

TABLE I: Parameters of some widely used profile models for the dark matter density in galaxies in Eq. (1). We also give the value of $\bar{J}(10^{-3})$, see text for details.

| | α | β | γ | R (kpc) | $\bar{J}(10^{-3})$ |
|-------|----------|---------|----------|---------|---------------------|
| Kra | 2.0 | 3.0 | 0.4 | 10.0 | 2.166×10^1 |
| NFW | 1.0 | 3.0 | 1.0 | 20 | 1.352×10^3 |
| Moore | 1.5 | 3.0 | 1.5 | 28.0 | 1.544×10^5 |
| Iso | 2.0 | 2.0 | 0 | 3.5 | 2.868×10^1 |

persion of high proper motion stars suggest the existence of a Super Massive Black Hole (SMBH) lying at the centre of our Galaxy, with a mass $\approx 2.6 \times 10^6 M_\odot$ [19].

It has been argued [20] that the process of adiabatic accretion of dark matter on the central SMBH would produce a “spike” in the dark matter density profile, leading to a power law index possibly as high as $\gamma \approx 2.4$. Although central spikes could be destroyed by astrophysical processes such as hierarchical mergers [21, 22], these dynamical destruction processes are unlikely to have occurred for the Milky Way [23]. The existence of such spikes would produce a dramatic enhancement of the annihilation radiation from the GC, and would allow to put stringent constraints on dark matter particles properties and distribution [20, 23, 24, 25].

As a first step for the study of indirect detection of KK dark matter, we choose to be conservative, and to focus on ordinary profiles without central spikes.

We now want to compute the observed flux from dark matter particle annihilation in the GC. The observed flux can be written as

$$\Phi_i(\psi, E) = \sigma v \frac{dN_i}{dE} \frac{1}{4\pi M^2} \int_{\text{line of sight}} ds \rho^2(r(s, \psi)) \quad (2)$$

where the index i denotes the secondary particle observed (we focus on γ -rays and neutrinos) and the coordinate s runs along the line of sight, in a direction making an angle ψ respect to the direction of the GC. σv is the annihilation cross section, dN_i/dE is the spectrum of secondary particles per annihilation and M is the mass of the LKP.

In order to separate the factors depending on the profile from those depending only on particle physics, we introduce, following [18], the quantity $J(\psi)$

$$J(\psi) = \frac{1}{8.5 \text{ kpc}} \left(\frac{1}{0.3 \text{ GeV/cm}^3} \right)^2 \int_{\text{line of sight}} ds \rho^2(r(s, \psi)) \quad (3)$$

We define $\bar{J}(\Delta\Omega)$ as the average of $J(\psi)$ over a spherical region of solid angle $\Delta\Omega$, centered on $\psi = 0$. The values of $\bar{J}(\Delta\Omega = 10^{-3})$ are shown in the last column of table I for the respective density profiles.

We can then express the flux from a solid angle $\Delta\Omega$ as

$$\Phi_i(\Delta\Omega, E) \simeq 5.6 \times 10^{-12} \frac{dN_i}{dE} \left(\frac{\sigma v}{\text{pb}} \right) \left(\frac{1 \text{ TeV}}{M} \right)^2 \bar{J}(\Delta\Omega) \times \Delta\Omega \text{ cm}^{-2} \text{s}^{-1} \quad (4)$$

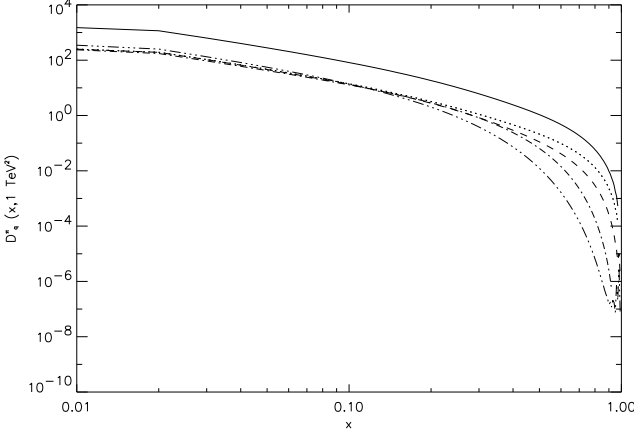


FIG. 1: Fragmentation function of different quark species into pions. From bottom to top, the curves are relative to quarks c and b (on the same curve, three dots-dashed line), s (dash-dotted), d (dashed), u (dotted) and sum of all (solid).

III. CROSS SECTIONS AND FRAGMENTATION FUNCTIONS

Annihilation cross sections of the LKP into Standard Model particles can be found in the appendix of [2]. Here we are concerned with the annihilation into fermions f which, in the non relativistic expansion limit ($\langle \sigma v \rangle \simeq a + bv^2$), is given by:

$$\sigma v(B^{(1)}B^{(1)} \rightarrow f\bar{f}) = \frac{\alpha_1^2 N_c N_f \pi Y^4}{9 M^2} (8 - v^2) \quad (5)$$

N_c , N_f and Y are respectively the number of colors, number of generations and hypercharge of fermion f . For neutrinos, we obtain

$$\langle \sigma v \rangle_{B^{(1)}B^{(1)} \rightarrow \nu\bar{\nu}} = 1.74313 \times 10^{-5} M^{-2} \quad (6)$$

per neutrino flavor. In addition to their direct production, neutrinos can also be produced via subsequent decay of charged pions $B^{(1)}B^{(1)} \rightarrow q\bar{q} \rightarrow \pi^\pm \rightarrow \nu + \dots$. Direct annihilation into two γ -rays is loop-suppressed, so high energy photons are mainly produced from decaying neutral pions $B^{(1)}B^{(1)} \rightarrow q\bar{q} \rightarrow \pi^0 \rightarrow \gamma\gamma$. To investigate the spectrum of secondary neutrinos and γ -rays, one has to go through the details of quark fragmentation into (neutral or charged) pions and their subsequent decay.

We use the Fragmentation Functions (FFs) described by Kretzer (2000) and implemented in [26]. In this approach the hadronisation of partons is described by the function $D_a^h(x, Q^2)$, which is the probability that the parton a fragments into a hadron h carrying a fraction x of the total momentum Q , where we sum over partons and anti-partons. For the processes we are considering $Q^2 \simeq M^2$.

In Fig. 1 we show the FFs relative to different quarks for the production of Pions.

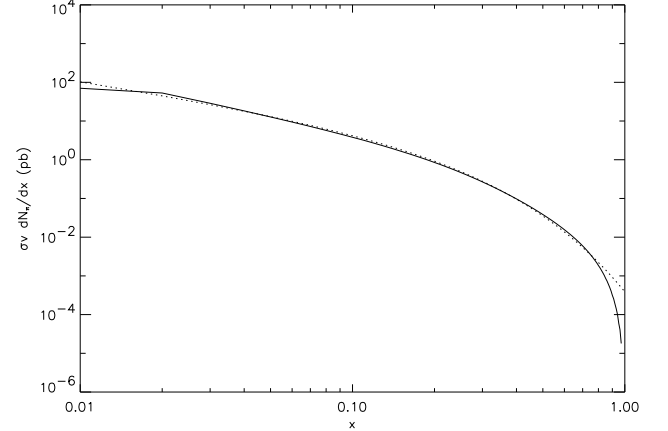


FIG. 2: Spectrum of charged pions after fragmentation times cross section (see Eq. (7), with $h = \pi^\pm$ and $Q^2 = 1 \text{ TeV}^2$). The dotted line is the analytic fit Eq. (8) which is sufficiently accurate up to $x \simeq 0.8$.

The spectrum of hadrons h produced after fragmentation is the sum of the FFs of the different quarks, weighted with the corresponding quark pair production cross sections in $B^{(1)}$ self-annihilation,

$$\sigma v \frac{dN_h}{dx} = \sum_a \sigma_a v D_a^h(x, Q^2). \quad (7)$$

The result for charged pions, $h = \pi^\pm$, is shown in Fig. 2 for $Q^2 = 1 \text{ TeV}^2$, along with the analytic fit

$$f(x) \simeq \frac{0.7}{x^{1.1} e^{7.5 x}} \text{ pb}, \quad (8)$$

which is sufficiently accurate up to $x \simeq 0.8$.

We are now able to compute the γ -ray spectrum resulting from neutral pion decay into two photons. The spectrum of photons from the decay of a single neutral pion is flat,

$$\frac{dN}{dE_\gamma} = \frac{2}{P_\pi} \quad (9)$$

for E_γ in the interval $(E_\pi \pm P_\pi)/2$, where E_i and P_i denote energy and momentum of the respective particle.

For relativistic pions, $E_\pi \simeq P_\pi$, so that the spectrum can be approximated with a Heavyside function. The γ -ray spectrum is thus

$$\frac{dN_\gamma}{dx} = \int_0^1 f(x') \frac{1}{x'} \theta(x' - x) dx'. \quad (10)$$

Examples of predicted fluxes for different particle masses and different density profiles are given in the next section.

Finally, to compute the neutrino spectra we use the formulae provided in [27]. In Fig. 3 we show the resulting spectra of γ -rays, e^+ , $\bar{\nu}_\mu$, ν_μ , and ν_e .

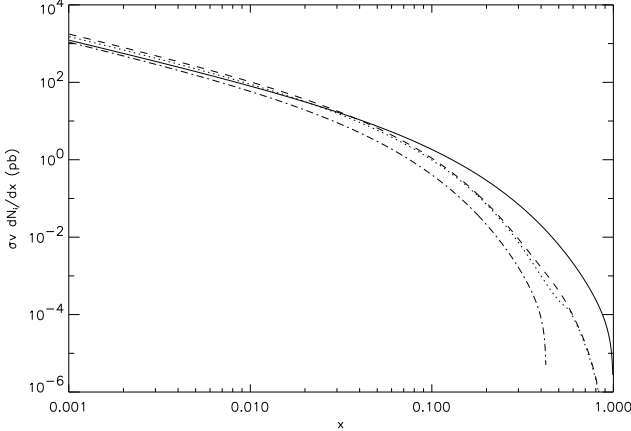


FIG. 3: The spectra of γ -rays (solid), e^+ (dashed), $\bar{\nu}_\mu$ (dotted), ν_e and $\bar{\nu}_\mu$ (dash-dotted), resulting from folding Eq. (7) with the pion decay spectra.

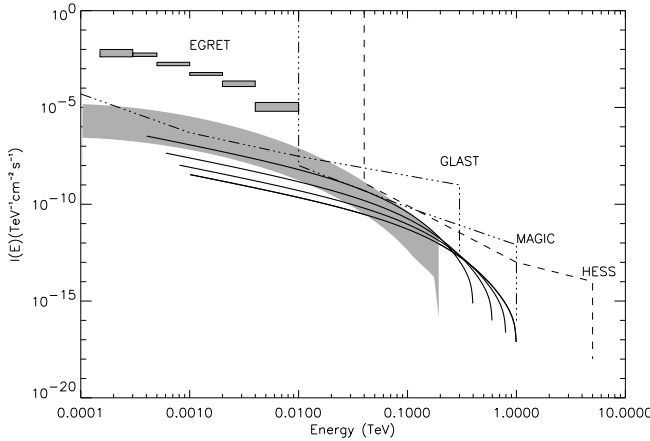


FIG. 4: Expected γ -ray fluxes for (top to bottom) $M = 0.4, 0.6, 0.8$, and 1 TeV and $\bar{J}(10^{-3}) = 500$. For comparison shown are typical γ -ray fluxes predicted for neutralinos of mass $\simeq 200 \text{ GeV}$, as well as EGRET data and expected sensitivities of the future GLAST, MAGIC and HESS experiments.

IV. GAMMA-RAY AND NEUTRINO FLUXES

In Fig. 4 we show the expected γ -ray flux in a solid angle $\Delta\Omega = 10^{-3}$ in the direction of the GC for $M = 0.4, 0.6, 0.8$, and 1 TeV and for $\bar{J}(10^{-3}) = 500$. To obtain the flux for a given profile, one can use the corresponding value of $\bar{J}(\Delta\Omega)$ given in the last column of Tab. I. In the same figure we show for comparison observational data from EGRET [28], and expected sensitivities of the future experiments GLAST [29], MAGIC [30] and HESS [31].

We notice that Eq. (4) can be written as

$$\Phi_l(\Delta\Omega) \simeq 5.6 \times 10^{-12} \frac{dN_l}{dE} \left(\frac{a}{\text{pb}} \right) \left(\frac{1 \text{ TeV}}{M} \right)^4 \bar{J}(\Delta\Omega) \times \Delta\Omega \text{ cm}^{-2} \text{ s}^{-1}. \quad (11)$$

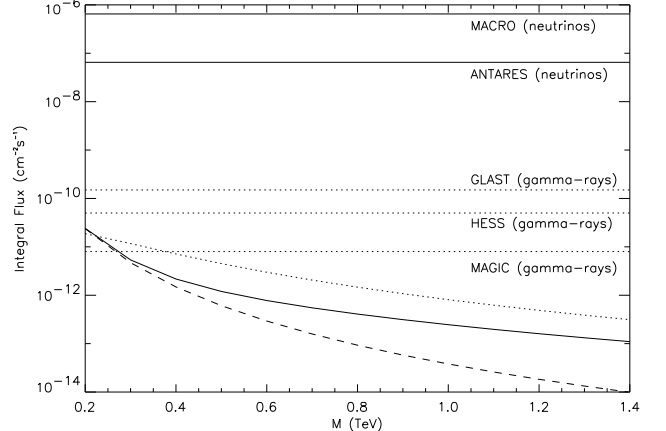


FIG. 5: Integral flux of γ -rays (dotted line) and muon neutrinos (solid) above 50 GeV . The dashed line shows the contribution of direct $B^{(1)}$ annihilation into neutrinos. Horizontal lines are sensitivities of present and future experiments for γ -rays (dotted horizontal lines) and neutrinos (solid horizontal lines).

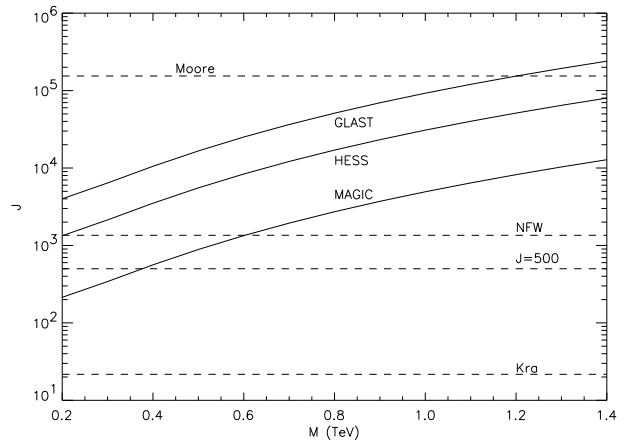


FIG. 6: Value of $J = \bar{J}(10^{-3})$ required to produce γ fluxes observable by the future GLAST, MAGIC and HESS experiments, as a function of the $B^{(1)}$ mass. For comparison we show the value of J for some profiles discussed in the text.

In this formula we used the fact that $B^{(1)}$ particles are expected to be non-relativistic in the GC, so we can safely use the non-relativistic limit of the cross section $\sigma v \rightarrow a(M/1\text{TeV})^{-2}$.

Given the particle physics details (cross sections and fragmentation) we are thus left with two free parameters: the mass of the dark matter particle, M , and the value of $\bar{J}(\Delta\Omega)$, depending on the specific dark matter profile adopted. We show in Fig. 6 the constraints on these two parameters based on the expected sensitivity of GLAST, MAGIC and HESS. For a NFW profile masses below 600 GeV are excluded if MAGIC does not observe any radiation from the GC.

Constraints from neutrino fluxes are weaker. High energy neutrinos can be detected with large underground telescopes, which are sensitive to muons originated by charged current interactions of ν_μ with the matter surrounding the detector. We used the above cited expressions for the charged pion decay obtained in Ref. [27], to compute the flux of secondary ν_μ on Earth.

In Fig. 5 we plot the integral flux of muon neutrinos above 50 GeV (solid line) as a function of the $B^{(1)}$ mass. This flux is obtained by adding the contribution of neutrinos directly produced by $B^{(1)}$ annihilations (dashed line), and secondary neutrinos originated by the decay of charged pions. We show in the same figure the MACRO experiment upper bound [32] for ν flux above 1 GeV from the GC (upper solid horizontal line) and a rough estimate of the sensitivity of ANTARES (lower solid) at the same energies (see e.g.[33]).

We show on the same plot the integral flux of photons (same threshold as for neutrinos, to compare relative flux) and the expected sensitivity of future experiments GLAST, MAGIC and HESS.

We also note that, following [10], the flux of high energy neutrinos from $B^{(1)}$ annihilations in the sun should be much higher, of the order of $10^{-7} \text{ cm}^{-2} \text{ s}^{-1}$. Note also that our estimate for the γ -ray flux is in good agreement with Fig. 3 of [5].

V. SYNCHROTRON RADIATION

Another interesting mean of indirect detection of dark matter is the synchrotron radiation originated from the propagation of secondary e^\pm in the Galactic magnetic field.

The magnetic field is supposed at equipartition (for details see [25]) in the inner part of the Galaxy and constant elsewhere. More specifically

$$B(r) = \max \left[1 \mu\text{G} \left(\frac{r}{\text{pc}} \right)^{-5/4}, 6 \mu\text{G} \right] \quad (12)$$

which means that the magnetic field is assumed to be in equipartition with the plasma out to a galactocentric distance $r_c = 0.23 \text{ pc}$, and to be equal to a typical value observed throughout the Galaxy at larger distances.

If the actual value of the magnetic field away from the central region was smaller than the one we considered, this would imply a shift of the radio spectrum towards lower energies and thus a higher flux for a given frequency. This would also translate into stronger constraints for the mass and annihilation cross section. Nevertheless we prefer to be conservative and consider a quite high value of B . Note that magnetic fields stronger than equipartition values are physically unlikely.

The synchrotron flux per solid angle at a given fre-

quency ν (cfr. Eq. (22) in [25]) is

$$L_\nu(\psi) \simeq \frac{1}{4\pi} \frac{9}{8} \left(\frac{1}{0.29\pi} \frac{m_e^3 c^5}{e} \right)^{1/2} \frac{\sigma v}{M^2} Y_e(M, \nu) \nu^{-1/2} I(\psi), \quad (13)$$

where

$$I(\psi) = \int_0^\infty ds \rho^2(r(s, \psi)) B^{-1/2}(r(s, \psi)), \quad (14)$$

and s is the coordinate running along the line of sight. $Y_e(M, \nu)$ is the average number of secondary electrons above the energy $E_m(\nu)$ of the electrons giving the maximum contribution at a given frequency ν and for a magnetic field B . We recall that (Eqs. (6) and (7) in [25])

$$E_m(\nu) = \left(\frac{4\pi}{3} \frac{m_e^3 c^5}{e} \frac{\nu}{B} \right)^{1/2}. \quad (15)$$

For frequencies around 400 MHz, used below, and for the lowest value of the magnetic field, we find that $E_m(400 \text{ MHz}) \lesssim 2 \text{ GeV}$. In reality, for dark matter profiles with central cusps, e.g. the NFW, Kravtsov, and Moore profiles discussed above, most of the annihilation signal comes from the inner region of the Galaxy, where the magnetic field is probably higher. In this case, and for $\nu = 400 \text{ MHz}$,

$$E_m(400 \text{ MHz}) = 5.0 \left(\frac{r}{\text{pc}} \right)^{5/8} \text{ GeV}, \quad (16)$$

which at the inner edge of the profile, corresponding to the Schwarzschild radius of the SMBH at the GC, $R_S = 1.3 \times 10^{-6} \text{ pc}$, takes the value $E_m(400 \text{ MHz}) = 8.8 \times 10^{-4} \text{ GeV}$. We thus always have $E_m(400 \text{ MHz}) \ll M$, which means that most of the secondary electrons are produced above this energy and contribute to the radio flux. We thus use the total electron multiplicity $Y_e(M)$ in the following.

For a particle of mass M , the product $\sigma v Y_e(M)$ is evaluated by adding the contribution of every annihilation channel i , with cross section $(\sigma v)_i$, producing $Y_e^i(M)$ electrons

$$\sigma v Y_e(M) = \sum_i (\sigma v)_i Y_e^i(M). \quad (17)$$

The main channels contributing to this flux are direct production of leptons, and annihilation into quarks, as discussed above. In the first case, we have $Y_e^{e^\pm}(M) = Y_e^{\mu^\pm}(M) \simeq 2$ in all the relevant range of masses, while in the quark channel, to count the number of electrons $Y_e^{q\bar{q}}(M)$, we integrate the FF for e^+ shown in Fig. (3), and multiply by a factor 2 to account for e^- from the corresponding decay of π^- . Using Eq. (17) and extrapolating the FF in Fig. (3) at low x values, we find e.g. $\sigma v Y_e(1 \text{ TeV}) \simeq 4 \times 10^{-3} \text{ TeV}^{-2}$, and $Y_e(1 \text{ TeV}) \simeq 8.4$ for $M = 1 \text{ TeV}$.

To obtain the observed radiation, one should multiply the luminosity L_ν with the synchrotron self-absorption

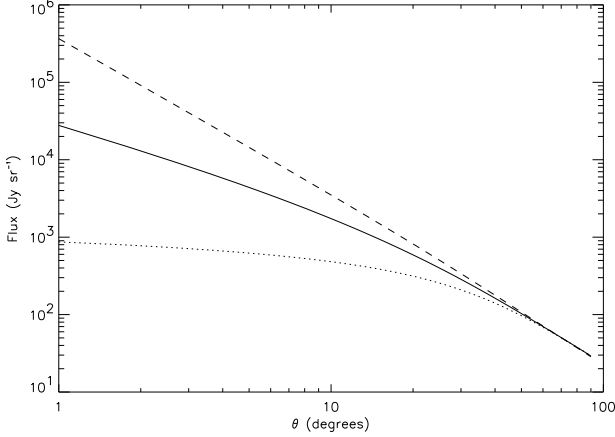


FIG. 7: Synchrotron emission at frequency $\nu = 327$ MHz for NFW (solid line), Kravtsov (dashed) and Moore (dotted) profiles, as a function of the angular distance from the Galactic center.

coefficient. In our case the optical depth is negligible and the self-absorption coefficient of the order of unity. In fact, using the expression introduced in [25], the optical depth can be expressed as

$$\tau \simeq \frac{\sigma v}{M^2} \frac{Y_e(M)}{4\pi} \frac{1}{\nu^3} \int_0^{d_\odot} ds \rho^2(s), \quad (18)$$

where $d_\odot \simeq 8$ kpc is the distance of the sun from the GC. Using $M = 1$ TeV, $\sigma v = 1.6 \times 10^{-4}$ TeV $^{-2}$ (cross section for annihilation into right-handed up quarks) and a NFW profile we find $\tau = 1.78 \times 10^{-4} (\nu/100\text{MHz})^{-3}$. We can thus neglect self-absorption unless the frequency considered is very small. For frequencies of the order of a few MHz the free-free absorption also sets in (see e.g. [34]).

In Fig. 7 we evaluate Eq. (13) for three different halo profiles, as a function of the angular distance from the GC.

To compare with observations we integrate over the relevant solid angle. The comparison between predicted and observed fluxes constrains the cross section of annihilating dark matter particles and therefore their mass. We studied three different cases:

1. Flux at $\nu = 408$ MHz in a cone of half-width 4 arcsec pointing towards the GC. Assuming a NFW profile, the comparison with the observed flux, which is $\lesssim 0.05$ Jy [35], puts the following constraint on the cross section

$$\sigma v \lesssim 7.7 \times 10^{-26} \left(\frac{M}{\text{TeV}} \right)^2 \frac{Y_e(1\text{TeV})}{Y_e(M)} \text{cm}^3 \text{s}^{-1}. \quad (19)$$

2. Flux at $\nu = 327$ MHz from a circular ring around the GC with inner and outer radius equal to 5 and 10 arcmin, respectively. We estimated the observed

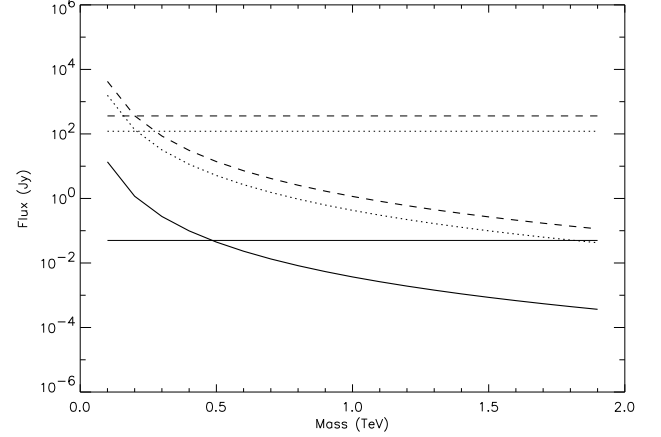


FIG. 8: Predicted (curves) and observed (horizontal lines) radio flux from regions close to the Galactic center, for a NFW profile, as a function of the particle mass. Bottom to top: case 1 (solid lines), case 2 (dotted lines) and case 3 (dashed lines), see text for details.

flux from [36] to be $\simeq 121$ Jy. If we impose the predicted flux for a NFW profile not to exceed the observations, then

$$\sigma v \lesssim 1.4 \times 10^{-24} \left(\frac{M}{\text{TeV}} \right)^2 \frac{Y_e(1\text{TeV})}{Y_e(M)} \text{cm}^3 \text{s}^{-1}. \quad (20)$$

3. Flux at $\nu = 327$ MHz in a cone of half-width 13.5 arcmin pointing towards the GC. The observed flux is $\simeq 362$ Jy [37]. The constraint on the cross section in this case is (for a NFW profile)

$$\sigma v \lesssim 1.6 \times 10^{-24} \left(\frac{M}{\text{TeV}} \right)^2 \frac{Y_e(1\text{TeV})}{Y_e(M)} \text{cm}^3 \text{s}^{-1}. \quad (21)$$

The constraints derived on the cross section are quite general and apply to any type of self-annihilating dark matter particles. To test specific candidates one has to specify the relation between cross section and mass. In particular the above constraints can be turned in a lower bound on the mass of the KK particle. In Fig. 8 we show predicted and observed fluxes for KK particles, for a NFW profile, as a function of the particle mass. For every case we plot the predicted and observed flux, the latter being of course represented by a horizontal line. Cases 1, 2 and 3 are respectively represented by solid, dashed and dotted lines. Case 1 is the most constraining, implying a lower bound on the mass of about 0.5 TeV.

To emphasize the importance of the density profile adopted, we plot in Fig. 9 the flux corresponding to case 1 for three different profiles. It is evident that for a Moore et al. profile the synchrotron flux would exceed the observed emission by several orders of magnitude for any interesting value of the $B^{(1)}$ mass, while for a Kravtsov profile $B^{(1)}$ particles are practically unconstrained.

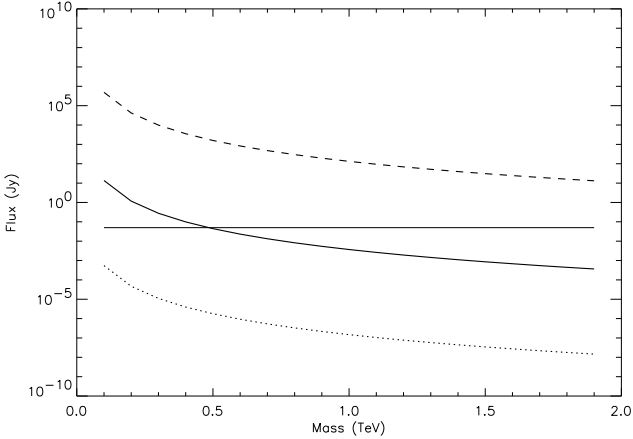


FIG. 9: Predicted radio flux from a 4 arcsec cone around the Galactic center, as a function of the KK particle mass for different density profiles. Bottom to top: Kravtsov et al. 2nd example (dotted line), NFW (solid line) and Moore et al (dashed line).

We also compared high latitude predicted fluxes with observations [34]. The strongest constraints result from the lowest frequencies at which free-free and synchrotron self-absorption are not yet important, i.e. around 10 MHz [34]. Here, the observed background emission between 0° and 90° from the Galactic anti-center is $\simeq 6 \times 10^6$ Jy. Comparing with the predicted emission results in the limit

$$\sigma v \lesssim 10^{-22} \left(\frac{M}{\text{TeV}} \right)^2 \frac{Y_e(1\text{TeV})}{Y_e(M)} \text{cm}^3 \text{s}^{-1}. \quad (22)$$

While this is considerably weaker than the constraints above, it is largely independent of the unknown GC dark matter profile.

Note that we can safely neglect other energy losses of secondary electrons such as Inverse Compton Scattering (ICS) and Pair Production (PP), which are much less efficient than synchrotron emission at the GC. Consider in fact the Synchrotron energy loss time

$$t_e \simeq E \left(\frac{dE}{dt} \right)^{-1} = \frac{3m_e^4}{2e^4 B^2 E}. \quad (23)$$

This implies a synchrotron photon energy density $u \simeq t_e \sigma v \rho^2 / M \lesssim 10^{-51} \text{GeV}^4$, compared to the cosmic microwave background energy density $u_{CMB} \simeq 10^{-51} \text{GeV}^4$. If σ_T is the Thomson cross section, we can express the ICS loss time as (see e.g. [38])

$$t_{ICS} \simeq \frac{3m_e^2}{4\sigma_T E u} \gtrsim 8 \times 10^{12} \left(\frac{\nu}{\text{MHz}} \right)^{-1/2} \text{pc}. \quad (24)$$

The energy loss time is even longer for PP, $t_{e+e-} \gtrsim 8.8 \times 10^{29} \text{pc}$.

Finally we can check whether we can get interesting constraints from clumped halos. In fact, high-resolution

N-body simulations suggest the existence of many substructures in the dark halos (see e.g. [17]). Without going into details, we refer to [39], where synchrotron emission is evaluated for neutralino annihilation in clumped halos.

If we consider clumps with a NFW profile, we can refer to Fig. 2 of [39] and extrapolate the flux for a 1 TeV neutralino at $\nu = 0.1$ GHz to be $\lesssim 10$ Jy, in a solid angle which we estimate, using the normalization of CMB anisotropies, to be around $\Delta\Omega = 3 \times 10^{-3}$ sr. We can have a rough idea of the flux corresponding to our clump candidate, for the same mass, by rescaling the flux by the ratio of the $B^{(1)}$ to the neutralino annihilation cross section. The expected flux for our candidate clump should thus be of the order of 100 Jy.

To see if this flux can outshine the background, we compare it with low frequency observations of the galactic anti-center regions for which recent estimates suggest a diffuse flux, at $\nu = 0.1$ GHz, of 3×10^5 Jy sr $^{-1}$ [40], which for the above solid angle would give a flux of $\approx 10^3$ Jy, thus exceeding the predicted flux by one order of magnitude. Thus the hypothesis of a clumped halo for our Galaxy does not put any further constraint on the parameters of our dark matter candidate.

VI. CONCLUSIONS

We have evaluated the prospects for indirect detection of $B^{(1)}$, the first Kaluza-Klein state of the Hypercharge B gauge boson. In particular, we focused on neutrino, γ -ray, and synchrotron fluxes from annihilation of $B^{(1)}$ particles in the Galactic halo.

Assuming a Galactic magnetic field at equipartition in the inner part of the Galaxy and equal a few micro Gauss elsewhere, we showed that, with the same density profile, synchrotron radiation give stronger constraints with respect to γ -ray emission while neutrino fluxes are much below the expected sensitivities of future experiments and several orders of magnitude smaller with respect to those expected from annihilations in the Sun.

Furthermore, synchrotron constraints are based on existing observations, while significant constraints on γ -rays will only result from hypothetic null searches at the expected sensitivity of future experiments like GLAST, MAGIC and HESS. On the other hand, predicted synchrotron fluxes are less robust because they not only depend on the dark matter profile close to the Galactic center, but also on specific assumptions for the Galactic magnetic field.

Comparing predicted and observed synchrotron fluxes from the Galactic center, we derived, for a NFW profile, an upper bound for the annihilation cross section of $\sigma v \leq 7.7 \times 10^{-26} (M/\text{TeV})^2 Y_e(1\text{TeV}) / Y_e(M) \text{cm}^3 \text{s}^{-1}$, which translates, for $B^{(1)}$ particles, into a lower bound on the mass of about $M \gtrsim 0.5$ TeV. We also discussed how this bound would vary depending on the dark matter profile adopted.

To conclude, the Minimal Supersymmetric Standard

Model is not the only viable extension of the Standard Model and the LSP is not the only viable Dark Matter candidate. It is therefore important to be open to other alternatives. Here, we focused on the Lightest Kaluza–Klein Particle, $B^{(1)}$, a typical WIMP and a viable DM candidate. Direct and indirect detection prospects for $B^{(1)}$ are challenging. In this work, we were able to set a constraint on the mass of the LKP and therefore on the compactification scale of Universal Extra Dimensions. Such a constraint comes from an existing measurement of synchrotron radiation and is more severe than the one from current electroweak precision tests. However, a better knowledge of the Galactic Dark Matter profile together with that of the magnetic field would be helpful to put this constraint on a more robust footing. The idea of

TeV Kaluza–Klein Dark Matter remains safe for a while.

Acknowledgements

This work is supported in part by the US Department of Energy, High Energy Physics Division, under contract W-31-109-Eng-38, by the David and Lucile Packard Foundation and also by the EU Fifth Framework Network "Supersymmetry and the Early Universe" (HPRN-CT-2000-00152). GB and GS would like to thank Joe Silk for many valuable discussions. GS thanks Carlos de Breuck for illuminating informations on radio observations.

- [1] T. Appelquist, H. C. Cheng and B. A. Dobrescu, Phys. Rev. D **64**, 035002 (2001) [arXiv:hep-ph/0012100].
- [2] G. Servant and T. M. Tait, arXiv:hep-ph/0206071. To be published in Nucl. Phys. B.
- [3] H. C. Cheng, K. T. Matchev and M. Schmaltz, Phys. Rev. D **66**, 036005 (2002) [arXiv:hep-ph/0204342].
- [4] T. Appelquist and H. U. Yee, arXiv:hep-ph/0211023.
- [5] H. C. Cheng, J. L. Feng and K. T. Matchev, arXiv:hep-ph/0207125.
- [6] G. Servant and T. M. Tait, arXiv:hep-ph/0209262.
- [7] H. V. Klapdor-Kleingrothaus, arXiv:hep-ph/0104028.
- [8] E. Aprile *et al.*, arXiv:astro-ph/0207670.
- [9] H. C. Cheng, K. T. Matchev and M. Schmaltz, Phys. Rev. D **66**, 056006 (2002) [arXiv:hep-ph/0205314].
- [10] D. Hooper and G. D. Kribs, arXiv:hep-ph/0208261.
- [11] A. Salucci, P. Borriello, MNRAS, **323**, 285 (2001)
- [12] F. C. van den Bosch and R. A. Swaters, arXiv:astro-ph/0006048.
- [13] J. J. Binney and N. W. Evans, arXiv:astro-ph/0108505.
- [14] A. Klypin, H. Zhao and R. S. Somerville, arXiv:astro-ph/0110390.
- [15] A. V. Kravtsov, A. A. Klypin, J. S. Bullock, J. R. Primack, Astrophys.J., **502**, 48 (1998) [arXiv:astro-ph/9708176].
- [16] J. F. Navarro, C. S. Frenk and S. D. White, Astrophys. J. **462** (1996) 563 [arXiv:astro-ph/9508025].
- [17] B. Moore, T. Quinn, F. Governato, J. Stadel and G. Lake, Mon. Not. Roy. Astron. Soc. **310** (1999) 1147 [arXiv:astro-ph/9903164].
- [18] L. Bergstrom, P. Ullio and J. H. Buckley, Astropart. Phys. **9** (1998) 137 [arXiv:astro-ph/9712318].
- [19] A. M. Ghez, B. L. Klein, M. Morris and E. E. Becklin, Astrophys. J. **509** (1998) 678 [arXiv:astro-ph/9807210].
- [20] P. Gondolo and J. Silk, Phys. Rev. Lett. **83** (1999) 1719 [arXiv:astro-ph/9906391].
- [21] P. Ullio, H. Zhao and M. Kamionkowski, Phys. Rev. D **64** (2001) 043504 [arXiv:astro-ph/0101481].
- [22] D. Merritt, M. Milosavljevic, L. Verde and R. Jimenez, Phys. Rev. Lett., **88**, (2002), 191301 [arXiv:astro-ph/0201376].
- [23] G. Bertone, G. Sigl and J. Silk, Mon. Not. Roy. Astron. Soc. accepted [arXiv:astro-ph/0203488.]
- [24] P. Gondolo, Phys. Lett. B **494** (2000) 181 [arXiv:hep-ph/0002226].
- [25] G. Bertone, G. Sigl and J. Silk, Mon. Not. Roy. Astron. Soc. **326**, 799 (2001) [arXiv:astro-ph/0101134].
- [26] S. Kretzer, Phys. Rev. D **62**, 054001 (2000) [arXiv:hep-ph/0003177]. FORTRAN routines available at the internet address www.pv.infn.it/radici/FFdatabase/parametrizations.html
- [27] S. Lee, Phys. Rev. D **58**, 043004 (1998) [arXiv:astro-ph/9604098].
- [28] H.A. Mayer-Haesselwander *et al.*, A&A 335, 161 (1998)
- [29] H. F. Sadrozinski, Nucl. Instrum. Meth. A **466** (2001) 292.
- [30] D. Petry [the MAGIC Telescope Collaboration], Astron. Astrophys. Suppl. Ser. **138** (1999) 601 [arXiv:astro-ph/9904178].
- [31] H. J. Volk, arXiv:astro-ph/0202421.
- [32] T. Montaruli [MACRO Collaboration], arXiv:hep-ex/9905020.
- [33] T. Montaruli [ANTARES Collaboration], arXiv:astro-ph/0207531.
- [34] H. V. Cane, Mon. Not. Roy. Astron. Soc. **189** (1979) 189
- [35] R.D. Davies, D. Walsh & R.S. Booth, Mon. Not. Roy. Astron. Soc. , **177** (1976) 319
- [36] K.R. Anantharamaiah, A. Pedlar, R.D. Ekers, W.M. Goss, Mon. Not. Roy. Astron. Soc. , **249** (1991) 262
- [37] T.N. La Rosa, N.E. Kassim, T.J. Lazio & S.D. Hyman, Astron. Journ. **119** (2000) 207
- [38] G.B. Rybicki, A.P. Lightman , Radiative Processes in Astrophysics, 1979, John Wiley & Sons
- [39] P. Blasi, A. V. Olinto and C. Tyler, arXiv:astro-ph/0202049.
- [40] R. Brown, in *Galactic and Extragalactic Radio Astronomy*, eds.: G. L. Verschuur and K. I. Kellermann (Springer, New York, 1974), p. 1.